PROCEEDINGS OF SCIENCE

ATLAS Experiment Overview and Higgs Searches

Richard Hawkings*
On behalf of the ATLAS Collaboration
CERN
E-mail: richard.hawkings@cern.ch

This document presents an overview of the status of the ATLAS experiment at the CERN Large Hadron Collider at the time of the July 2012 ICHEP conference in Melbourne, with a strong focus on the search for the Standard Model Higgs boson. The final results from the 2011 dataset are presented, together with first results in the $H \to \gamma\gamma$ and $H \to ZZ^{(*)} \to 4\ell$ channels from the 2012 dataset, using the 5.8 fb^{-1} of pp collision data taken at $\sqrt{s} = 8$ TeV that were available at the time of the conference. Combining both 2011 and 2012 data, a significant excess of events is seen in the Higgs search at a mass of around 126 GeV. This excess is interpreted as evidence for a new, narrow resonance, consistent with the production and decay of the Standard Model Higgs boson.

36th International Conference on High Energy Physics,
July 4-11, 2012
Melbourne, Australia

*Speaker.

PoS(ICHEP2012)006

1. Introduction

One of the primary goals for the first phase of the LHC physics program is the search for the Standard Model (SM) Higgs boson. Preliminary analysis of the 2011 ATLAS data taken at $\sqrt{s} = 7$ TeV showed hints for a possible Higgs boson-like object around a mass m_H of 126 GeV with a combined local significance of 2.5σ, with the excess concentrated in the $H \to \gamma\gamma$ and $H \to ZZ^{(*)} \to 4\ell$ channels [1]. Similar hints were also seen by the CMS Collaboration [2]. After the restart of LHC data-taking at $\sqrt{s} = 8$ TeV in April 2012, both experiments looked forward to investigating these features in more detail as soon as possible.

The performance of ATLAS [3] in the initial 2012 data-taking up to mid-June is briefly reviewed in Section 2. During this period, ATLAS also finalised the main SM Higgs boson searches with the 2011 data, as discussed below in Section 3, and performed additional searches for SM and other Higgs bosons, some of which are summarised in Section 4. The status of the SM Higgs search with 2012 data at the time of the conference is described in detail in Section 5, with a focus on the $H \to \gamma\gamma$ and $H \to ZZ^{(*)} \to 4\ell$ channels. Conclusions are given in Section 6.

2. ATLAS data-taking in 2012

Physics data-taking with pp collisions at $\sqrt{s} = 8$ TeV started in early April and ended at the first LHC technical stop on 18th June. During this period, ATLAS recorded 6.3 fb^{-1} of data with 95 % data-taking efficiency. Of this sample, 93.6 % passes data quality cuts in all sub-detectors, giving 5.8 fb^{-1} for typical analysis selections; this fraction will be improved slightly after reprocessing later this year.

The LHC delivered physics fills with peak instantaneous luminosity of up to 7×10^{33} cm^{-2}s^{-1}, corresponding to 30–35 superimposed minimum bias pp collisions in each bunch crossing at the start of fills. The ATLAS trigger and offline reconstruction algorithms were extensively optimised during the 2011–12 winter shutdown to make them robust against such high levels of pileup, beyond the design specifications of the detector. The trigger menu was optimised to give a 65 kHz level-1 trigger rate at the start of fill, and a fill-averaged event filter output rate of 400 Hz. Typical trigger thresholds at the event filter are 24 GeV transverse momentum for single isolated electrons and muons, 8–18 GeV for dileptons, 20–35 GeV for diphotons, 20–29 GeV for di-taus and 80 GeV for missing transverse momentum $E_T^{\rm miss}$. The offline event reconstruction at Tier-0 takes from 15–40 s/event, and was run on up to 7 500 CPU cores in parallel to keep up with the data-taking rate. Up to 200 Hz of additional data for hadronic final states and B-physics was recorded in 'delayed streams', and will be processed offline once the 2012 data-taking run has finished. The worldwide Grid computing effort supporting ATLAS continues to be vital, with 150 000 simultaneous Monte Carlo simulation and user analysis jobs being run routinely.

3. SM Higgs boson searches with the 2011 data

Within the Standard Model, the phenomenology of Higgs boson production and decay is precisely predicted, once the Higgs mass is known. The production is dominated by gluon-gluon fusion, with smaller contributions from vector boson fusion (VBF, where two W or Z bosons radiated

Channel	m_H range (GeV)	Reference
$H \to \gamma\gamma$	110-150	[5]
$H \to ZZ^{(*)} \to 4\ell$	110-600	[6]
$H \to ZZ \to \ell^+\ell^- q\bar{q}$	200–280–600	[7]
$H \to ZZ \to \ell^+\ell^- \nu\bar{\nu}$	200–300–600	[8]
$H \to WW^{(*)} \to \ell^+\nu\ell^-\bar{\nu}$	110–200–300–600	[9]
$H \to WW \to \ell\nu q\bar{q}$	300–600	[10]
$H \to \tau^+\tau^- \to \ell^+\ell^-, \ell\tau_{\rm h}, \tau_{\rm h}\tau_{\rm h}$	110–150	[11]
$WH \to \ell\nu b\bar{b}$; $ZH \to \ell^+\ell^- b\bar{b}$, $\nu\bar{\nu}b\bar{b}$	110-130	[12]

Table 1: Summary of ATLAS SM Higgs searches performed with the 2011 data, showing the decay channel, mass range and analysis references. Multiple mass ranges indicate points where the analysis changes significantly.

from initial quarks fuse to make a Higgs boson), associated production of a Higgs boson together with a W or Z boson (WH and ZH), and a very small contribution from Higgs boson production in association with a top-quark pair ($t\bar{t}H$). The decay modes vary with m_H, being dominated by $H \to b\bar{b}$ at low mass, with $H \to WW^{(*)}$ becoming dominant as the WW threshold is crossed. The rarer $H \to ZZ^{(*)}$ and $H \to \gamma\gamma$ modes are also important due to their clean experimental signatures.

The different production and decay modes give rise to a rich experimental phenomenology, with many different analysis channels being used to cover the full mass range of interest, as shown in Table 1. The individual analyses are combined using a dedicated likelihood-based procedure, which takes into account signal and control regions from each analysis and correlations between the analyses [4]. The compatibility with or exclusion of particular SM Higgs mass hypotheses are tested by scaling the predicted Higgs boson contribution in the likelihood fit by a signal strength parameter μ, applied coherently to all channels. The exclusion of $\mu = 1$ at a particular Higgs mass hypothesis corresponds to the exclusion of the production of a SM Higgs boson at that mass.

The 95 % confidence level (CL) exclusion limits obtained with the complete 2011 dataset are shown in Figure 1. With this dataset, the expected exclusion is 120–560 GeV, whereas the Higgs mass regions 111.4–116.6 GeV, 119.4–122.1 GeV and 129.2–541 GeV are actually excluded. The region around 126 GeV cannot be excluded, due to excesses of events in the $H \to \gamma\gamma$ and $H \to ZZ^{(*)} \to 4\ell$ channels. This effect can be quantified using the local p_0 value, the probability that a background-only experiment would fluctuate to produce a signal-like result as least as significant as that observed in data. The local p_0 is shown as a function of m_H in Figure 2 (left). The observed local p_0 values are 2.8 ($\gamma\gamma$), 2.1 (4ℓ) and 2.9σ (combination of all channels), and the corresponding expected values for this dataset with a 126 GeV SM Higgs boson are 1.4, 1.4 and 2.9σ. Although intriguing, the global probability to see a combined excess at least as significant as this anywhere in the mass range 110–600 GeV, after taking the 'look elsewhere effect' or 'trials factor' into account is about 15 %, corresponding to 1σ. The best-fit signal strengths for the different channels at m_H values of 119, 126 and 130 GeV are shown in Figure 2 (right); note that the error bars correspond to intervals in the likelihood ratio $\lambda(\mu)$ of $-2\ln\lambda(\mu) < 1$, which correspond only approximately to 1σ.

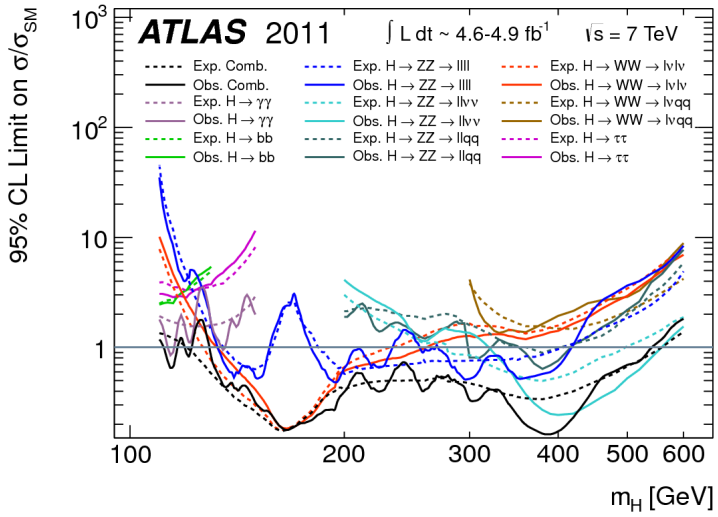

Figure 1: The observed (solid) and expected in absence of signal (dashed) 95 % CL limits on the Higgs boson production cross-section scaled to that of the Standard Model, as a function of m_H for the individual search channels and combination, using the 2011 ATLAS dataset [4].

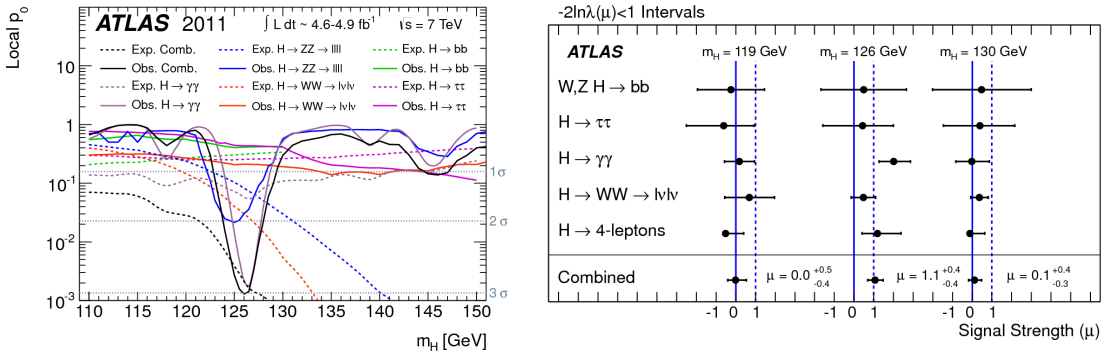

Figure 2: Left: Compatibility with the background-only hypothesis p_0 for the individual search channels and their combination as a function of m_H, together with expected p_0 values assuming a SM Higgs boson of mass m_H. Right: Best fit signal strength μ for individual search channels and their combination, for different assumed m_H [4].

4. Other Higgs boson searches with the 2011 data

Dedicated searches for the associated Higgs boson production mode WH probe a different production mechanism, and have high sensitivity to the HWW coupling, especially in the $H \to WW^{(*)}$ decay channel. A search for $WH \to WWW^{(*)} \to \ell\nu\ell\nu\ell\nu$ was performed using the 2011 dataset, by looking for final states with three charged leptons and large $E_T^{\rm miss}$ [13]. No excess was seen, and limits were set in the mass range 110–300 GeV at production rates between 2.7 (at $m_H = 165$ GeV) and 43 times the SM expectation.

In the Minimal Supersymmetric Standard Model, there are two Higgs doublets giving rise to three neutral Higgs bosons h, H and A, denoted generically by ϕ. The dominant production

mechanisms are gluon-gluon fusion, and production in association with a $b\bar{b}$-pair, particularly at high $\tan\beta$. The main decay modes are $\phi \to b\bar{b}$ (with 90 % branching ratio), $\phi \to \tau^+\tau^-$ (10 %), and $\phi \to \mu^+\mu^-$ (0.04 %), only the latter two being feasible discovery channels. Both decay modes were utilized in searches in both b-tagged and b-vetoed samples with the complete 2011 dataset [14]. No evidence of Higgs boson production was seen, and limits were set on the product of cross-sections and branching ratios, and in the $(m_A, \tan\beta)$ plane in the $m_{\rm h}^{\rm max}$ scenario with $\tan\beta > 0$.

5. SM Higgs boson search with the 2012 data

As can be seen from the expected limit curves in Figure 1, the most sensitive channels around $m_H = 126\,\text{GeV}$ are $H \to WW^{(*)} \to \ell^+\nu\ell^-\bar{\nu}$, $H \to \gamma\gamma$ and $H \to ZZ^{(*)} \to 4\ell$. The latter two have good mass resolution and are expected to show a signal peak over a smoothly-varying background. They also rely on the reconstruction of photons, electrons and muons, which are among the easier physics objects to reconstruct in a high-pileup environment. ATLAS therefore gave priority to these two channels for early 2012 data analysis, reoptimising the analyses used in 2011 for high pileup and low m_H. These optimisations were based on Monte Carlo studies and data control regions in the 2011 data, and all analysis techniques and selection cuts were fixed before looking at the 2012 data, as discussed in more detail in Sections 5.1 and 5.2 below.

The $H \to WW^{(*)} \to \ell^+\nu\ell^-\bar{\nu}$ channel is also statistically powerful in this mass region, but the signal would appear as a broad excess in the transverse mass distribution as the two neutrinos cannot be reconstructed. The background evaluation requires an excellent understanding of $E_T^{\rm miss}$, jets and b-tagging, all of which are difficult in a high pileup environment. Extensive studies of control regions in 2012 data were needed before looking at the signal region, and first results in this channel were not yet available at the time of this conference.

5.1 Analysis of the $H \to \gamma\gamma$ channel

The Higgs boson signal in the $H \to \gamma\gamma$ channel appears as narrow peak in the $m_{\gamma\gamma}$ distribution on top of a slowly varying background. The background level and shape can be fitted from the data, which are divided into several analysis categories with different $m_{\gamma\gamma}$ resolution and signal/background ratios depending on the properties of the selected photons in each event. The background comes mainly from irreducible continuum $\gamma\gamma$ production and γ-jet production with one jet misidentified as an isolated photon, with a smaller contribution from jet-jet events.

During the 2011–12 winter shutdown, the analysis was extensively reoptimised, as described in detail in Ref. [15]. The kinematic requirements were optimised, raising the cut on the p_T of the second photon from 25 to 30 GeV (the first photon is required to have $p_T > 40\,\text{GeV}$). A new neural network-based photon identification algorithm with better efficiency for the same background rejection was introduced for the 2011 data. For 2012 data, a cut-based photon identification, optimised for stable performance with high pileup, was used. The photons are required to be isolated, requiring the transverse energy sum of all positive-energy topological calorimeter clusters in a cone of $\Delta R = 0.4$ around the photon direction to be less than 4 GeV. The use of topological clusters rather than calorimeter cells used previously improves the stability against pileup.

A new '2-jet' analysis category was introduced, selecting events with at least two $p_T > 25$–30 GeV jets separated by $\Delta\eta_{\rm jj} > 2.8$ and having $m_{\rm jj} > 400\,\text{GeV}$. As shown in Figure 3 (left), such

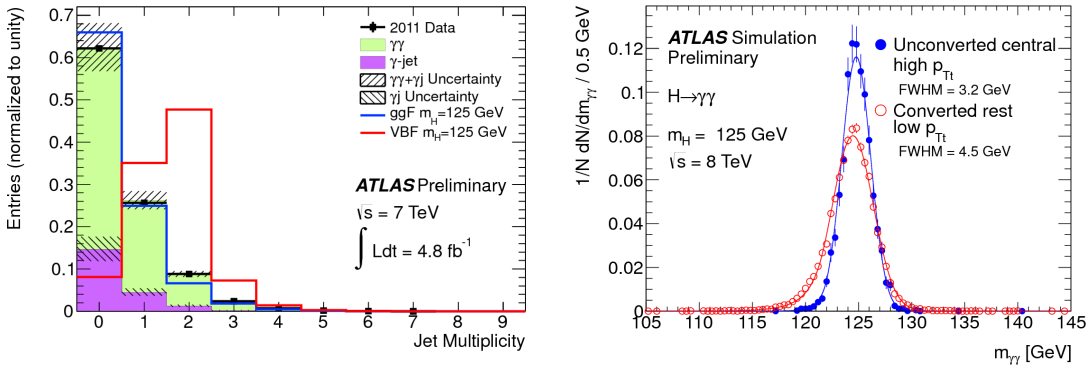

Figure 3: Left: Jet multiplicity in the selected $\sqrt{s} = 7$ TeV data compared to simulation, showing the expected distributions for background together with gluon-gluon fusion and VBF Higgs boson signal contributions. Right: Simulated $m_{\gamma\gamma}$ invariant mass distributions at $\sqrt{s} = 8$ TeV for two event categories with high and low resolutions [15].

events are expected to be enriched in VBF Higgs boson production compared to the background and gluon-gluon Higgs boson production which peak at low jet multiplicity. The remaining events were classified into nine separate categories, depending on whether the photons were reconstructed as converted or unconverted candidates, their η-positions within the calorimeter, and the transverse momentum of the diphoton system with respect to the event thrust axis (p_{Tt}).

To reconstruct the $\gamma\gamma$ invariant mass, the photon angles were determined using a combination of longitudinal segmentation in the liquid-argon electromagnetic calorimeter ('photon pointing'), and the reconstructed photon conversion vertex (where available), giving a $\gamma\gamma$ z-vertex position resolution of about 15 mm. This information was combined with primary vertex information from the inner detector tracking to associate jets to the correct primary vertex in the 2-jet category. The expected invariant mass spectrum for $H \to \gamma\gamma$ decays was modelled using a combination of Gaussian and Crystal Ball functions, and the full-width half-maximum resolution varies from 3 to 6 GeV depending on the event category, as shown in Figure 3 (right).

The $m_{\gamma\gamma}$ distribution in each category was fitted using the signal function discussed above together with a background function whose parameters were fitted to the data. The choice of background function for each category was selected from amongst 4th-order Bernstein polynomials, exponentials of 2nd-order polynomials or a simple exponential, based on extensive studies of high-statistics simulated samples of $\gamma\gamma$, γ-jet and jet-jet events, taking into account the potential bias and fit stability given the expected data statistics in each category. The residual biases on a potential 125 GeV signal seen in background-only simulation studies were taken as systematics on the fitted signal yield in data.

The inclusive $m_{\gamma\gamma}$ distribution combining the 23 788 selected events from the 2011 data and 35 271 events from the 2012 data, before separation into the ten analysis categories, is shown in Figure 4. A fit to a 4th-order Bernstein polynomial background and a signal component at 126.5 GeV shows a significant excess at this mass. However, the full analysis results are obtained by fitting the $m_{\gamma\gamma}$ distributions of the ten categories separately with a common signal strength. The 95 % CL limits obtained from the ten-category fit are shown in Figure 5 (left). In the absence of

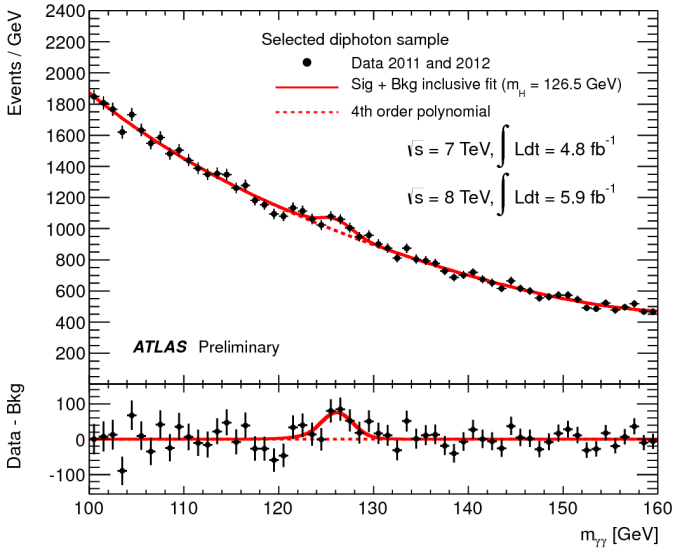

Figure 4: $m_{\gamma\gamma}$ distribution for the combined 2011+2012 data sample, together with a fit incorporating background and 126.5 GeV signal components. The lower plot shows the residuals of the data with respect to the fitted background [15].

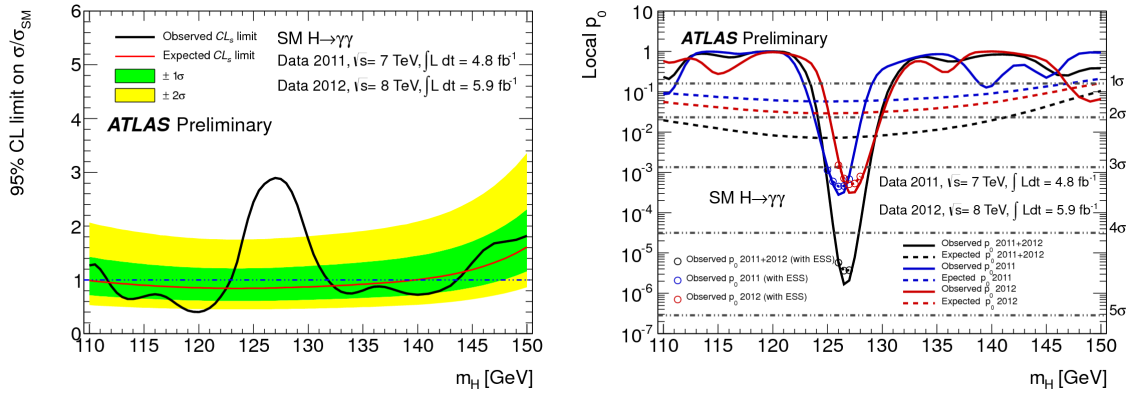

Figure 5: Left: Observed and expected limits on the $H \to \gamma\gamma$ production rate with respect to the SM prediction as a function of m_H. Right: Compatibility with the background-only hypothesis p_0 together with the value expected for a SM Higgs boson of mass m_H, showing results from 2011 and 2012 data individually and combined [15].

signal, an exclusion of SM Higgs boson masses in the range 110–139.5 GeV is expected with this dataset. The observed exclusion is from 112–122.5 GeV and 132–143 GeV, and the region around 126 GeV shows a significant excess. As shown in Figure 5 (right), the most significant deviation from the background-only hypothesis occurs at $m_H = 126.5$ GeV, with a local significance of 4.7σ, with similar-sized excesses in both 2011 and 2012 data at compatible masses. The significance of the combined excess is reduced to 4.5σ after taking the effect of the 0.6 % systematic uncertainty on the photon energy scale into account.

The fitted signal strength μ is shown as a function of m_H in Figure 6 (left), and is 1.9 ± 0.5 at 126.5 GeV, higher than but still compatible with the rate expected in the SM ($\mu = 1$). The

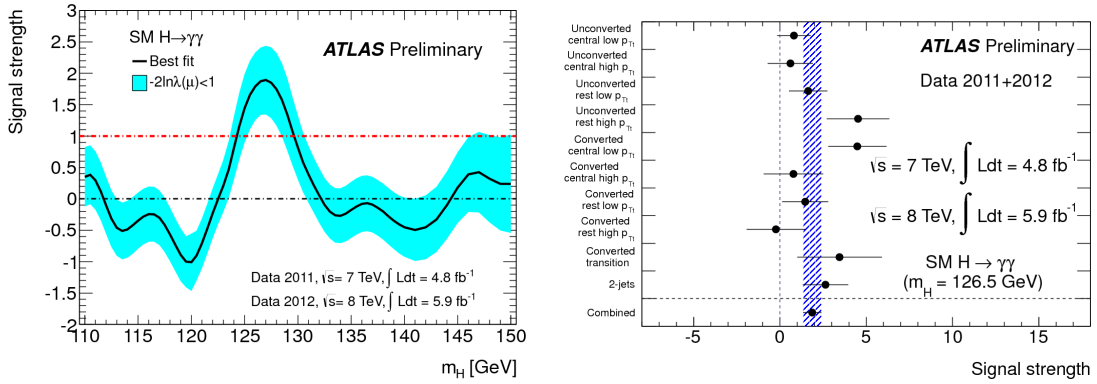

Figure 6: Left: Fitted signal strength μ for $H \to \gamma\gamma$ as a function of m_H. Right: Fitted signal strength at $m_H = 126.5$ GeV for the ten analysis categories individually and combined [15].

breakdown as a function of analysis categories is given in Figure 6 (right), showing that the excess is robust and distributed across several of the categories, including the 2-jet category.

5.2 Analysis of the $H \to ZZ^{(*)} \to 4\ell$ channel

In the $H \to ZZ^{(*)} \to 4\ell$ channel [16], the Higgs boson signal appears as a narrow peak in the four-lepton invariant mass distribution over a background dominated by continuum $ZZ^{(*)}$ production, with $Zq\bar{q}$, $Zb\bar{b}$ and $t\bar{t}$ also being important at low m_H. The small branching ratios involved mean that only a few candidates are expected, so the reconstruction efficiency for low-p_T leptons is particularly important. Before analysing the 2012 data, the kinematic selections were reoptimised to increase the sensitivity at low m_H. For 2012 data, improved electron reconstruction and identification algorithms were used, allowing for the effects of electron bremsstrahlung in the track pattern recognition, improving the stability against pileup and refitting the final tracks with a Gaussian Sum Filter algorithm to account for energy losses in the track fit; the last improvement was also applied in 2011 data. Small improvements were also made to increase the muon reconstruction coverage. The kinematic selections require four leptons with minimum p_T requirements ranging from 20 to 6 GeV, and cuts are made on the invariant mass of the leading (m_{12}) and sub-leading (m_{34}) lepton pairs. The leading pair was constrained to the Z-boson mass for $m_{4\ell} < 190$ GeV, and both lepton pairs were constrained for high $m_{4\ell}$. The resulting invariant mass resolution varies from 1.8 GeV (4μ) to 2.5 GeV ($4e$) for $m_H = 130$ GeV, as shown in Figure 7 (left). The corresponding combined reconstruction and selection efficiency was improved from 27 % for the old 2011 analysis at $\sqrt{s} = 7$ TeV to 41 % for the new 2012 analysis at $\sqrt{s} = 8$ TeV in the 4μ channel, and from 14 % to 23 % in the $4e$ channel.

The estimate of the $ZZ^{(*)}$ continuum background was taken from simulation, but the rates of $Zq\bar{q}$, $Zb\bar{b}$ and $t\bar{t}$ were normalised using data control regions. When the sub-leading lepton pair is $\mu^+\mu^-$, only the latter two backgrounds are important, and a $b\bar{b}$-enriched control region with relaxed isolation cuts on these leptons was used, as shown in Figure 7 (right). When the sub-leading lepton pair is e^+e^-, $Zq\bar{q}$ events with contributions from photon conversions and misidentified hadrons are also important, and the normalisation was obtained using high-threshold transition radiation tracker hits, innermost pixel layer hit and calorimeter shape information in a relaxed selection.

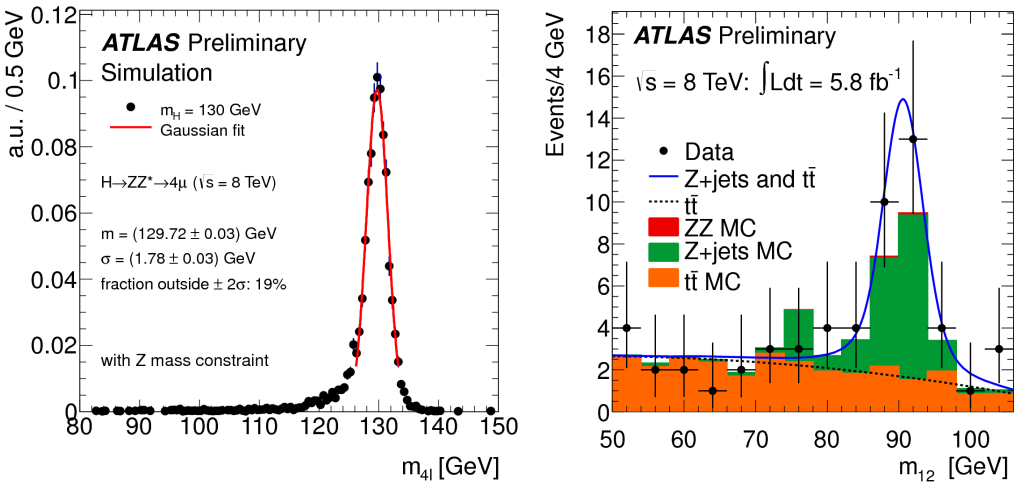

Figure 7: Left: Invariant mass distribution for simulated $H \to ZZ^{(*)} \to 4\mu$ events with $m_H = 130\,\text{GeV}$ at $\sqrt{s}$ =8 TeV. Right: Distribution of m_{12} for the control region with looser requirements on sub-leading muons, for $\sqrt{s} = 8\,\text{TeV}$ data together with the background fit and expectations from simulation [16].

$m_{4\ell}$ range	110–160 GeV			160–600 GeV			120–130 GeV		
$\sqrt{s} = 7, 8$ TeV	4μ	$2e2\mu$	$4e$	4μ	$2e2\mu$	$4e$	4μ	$2e2\mu$	$4e$
Background	11.8	12.7	9.6	45.8	71.1	29.8	1.3 ± 0.1	2.2 ± 0.2	1.6 ± 0.2
$m_H = 125\,\text{GeV}$	2.4	2.7	1.2	-	-	-	2.1 ± 0.3	2.3 ± 0.3	0.9 ± 0.1
Data	12	16	11	59	89	43	6	5	2

Table 2: Expected numbers of background and signal (for $m_H = 125\,\text{GeV}$) events in the different $H \to ZZ^{(*)} \to 4\ell$ channels, shown separately for low ($m_{4\ell} < 160\,\text{GeV}$) and high ($m_{4\ell} > 160\,\text{GeV}$) mass candidates, and for events in the 120–130 GeV mass window [16].

The number of selected candidates in data is compared to the expectations for backgrounds and a 125 GeV Higgs boson signal in Table 2. The $m_{4\ell}$ distributions for low mass candidates at 8 and 7 TeV are shown in Figure 8. An excess of events compatible with SM Higgs boson production is visible around 125 GeV, particularly in the 4μ and $2e2\mu$ channels. The observed and expected excluded cross-sections are also shown in Figure 8; the expected exclusion in the absence of a signal is 124–164 GeV and 176–500 GeV, and the observed exclusions are 131–162 GeV and 170-460 GeV.

The compatibility of the $H \to ZZ^{(*)} \to 4\ell$ results with the background-only hypothesis is shown in Figure 9 (left); the most significant deviation occurs at $m_H = 125\,\text{GeV}$ with a p_0 corresponding to 3.4σ, with contributions from both 2011 and 2012 data. As shown in Figure 9 (right), the fitted signal strength μ is compatible with one around this mass.

5.3 Results of the combined search

The results of the updated 2011 and 2012 data analyses in the $H \to \gamma\gamma$ and $H \to ZZ^{(*)} \to 4\ell$ channels were combined with the existing 2011 data analyses in the other channels listed in Table 1 [17]. The resulting 95 % CL exclusion as a function of m_H is shown in Figure 10. With this dataset,

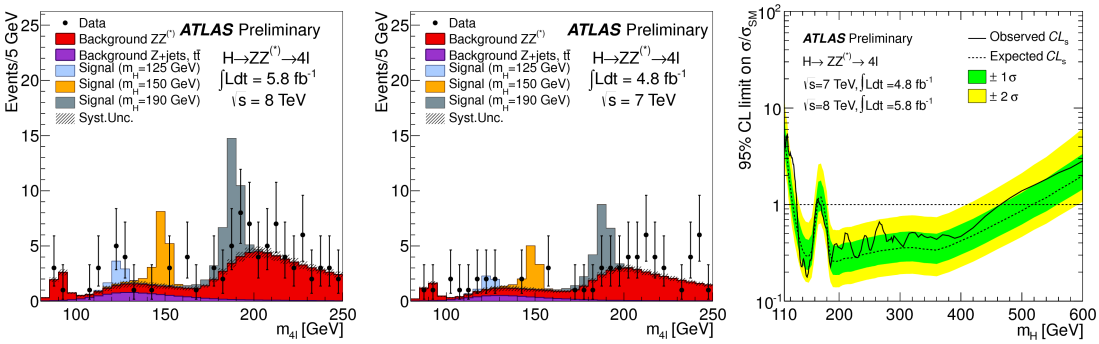

Figure 8: Four-lepton invariant mass distributions for selected candidates in the low mass region in the $\sqrt{s} =$ 8 TeV (left) and 7 TeV (centre) data samples. Right: Observed and expected limits on the $H \to ZZ^{(*)} \to 4\ell$ production rate with respect to the SM prediction as a function of m_H [16].

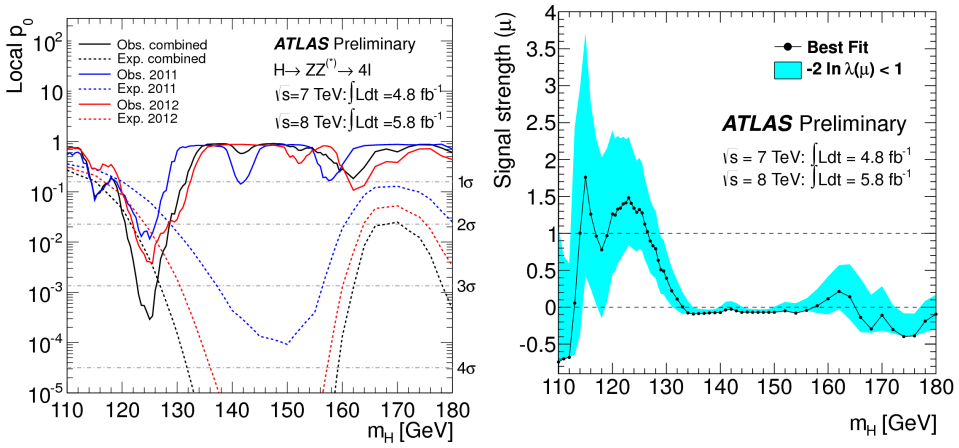

Figure 9: Left: Compatibility with the background-only hypothesis p_0 for the $H \to ZZ^{(*)} \to 4\ell$ 2011 and 2012 individual and combined analyses, together with the expected values for SM Higgs boson production at each m_H value. Right: Fitted signal strength μ as a function of m_H [16].

the mass range from 110–582 GeV would be expected to be excluded if no SM Higgs boson were present, but the observed exclusion covers only 110–122.6 GeV and 129.7–558 GeV, with most of this region being excluded at 99 % CL. The compatibility with the background-only hypothesis is shown in Figure 11, and the most significant deviation (smallest local p_0) corresponds to 5.1σ, at $m_H = 126.5$ GeV, close to the expected significance for a SM Higgs boson at this mass of 4.6σ. The excess is mildly sensitive to systematic uncertainties on the energy scale and resolution for photons and electrons, which reduce the significance to 5.0σ. Considering the look-elsewhere effect in the entire search mass range from 110–600 GeV gives a global significance of 4.1σ. Combining the 2012 $\gamma\gamma$ and 4ℓ data alone gives a maximum local significance of 4.0σ at 127 GeV, corresponding to a global significance of 3.1σ when considering the mass range 110–130.7 GeV which was not excluded at 99 % with the 2011 data analysis.

The signal strength measured in the different channels is shown in Figure 12 (left). Of the three most sensitive channels, significant signals are seen in $H \to \gamma\gamma$ and $H \to ZZ^{(*)} \to 4\ell$ whilst

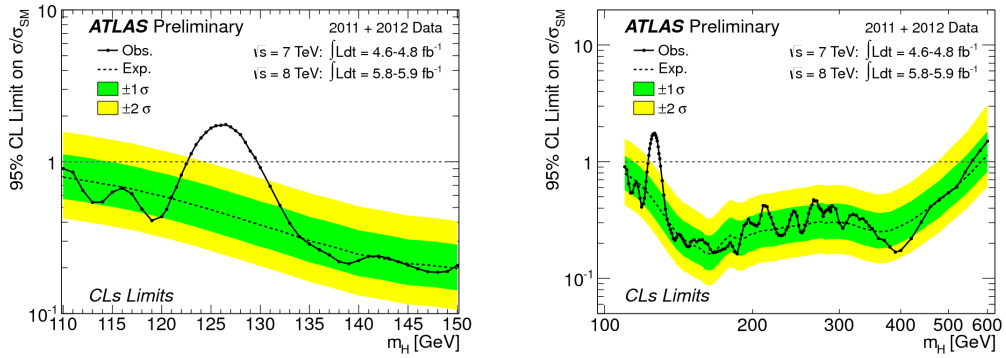

Figure 10: Observed and expected exclusion limits on SM Higgs production from the combined analysis, in the low (left) and full (right) Higgs boson mass ranges [17].

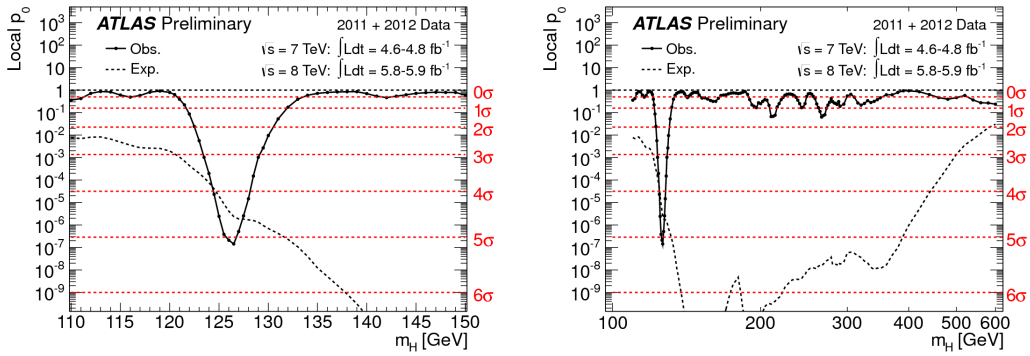

Figure 11: Compatibility with the background-only hypothesis p_0 for the combined analysis, in the low (left) and full (right) Higgs boson mass ranges. The expected p_0 for SM Higgs boson production at each m_H value is also shown [17].

$H \to WW^{(*)} \to \ell^+\nu\ell^-\bar{\nu}$ (where only the 2011 data has been analysed) is compatible with both $\mu = 0$ and $\mu = 1$. The combination of all channels gives a signal strength of $\mu = 1.2 \pm 0.3$, consistent with the SM expectation of $\mu = 1$. The consistency of the signals in $\gamma\gamma$ and 4ℓ modes is explored in Figure 12 (right), which shows two-dimensional contour plots when both m_H and μ are left free to float, independently for each channel. The best-fit masses from the two channels are compatible, and energy-scale systematics have only a small effect on the contours.

6. Conclusions

The last few months have been a very interesting and busy time for ATLAS. The 2012 data-taking is proceeding very well, and the collaboration is very grateful to the LHC and other CERN teams for the excellent machine performance. Many new measurements and new physics searches have been performed using the 2011 and early 2012 data, but so far without giving any hints of physics beyond the Standard Model.

However, ATLAS has observed a significant excess of events in the search for the Standard Model Higgs boson, with excesses around $m_H = 126.5$ GeV of 4.5 and 3.4σ local significance in

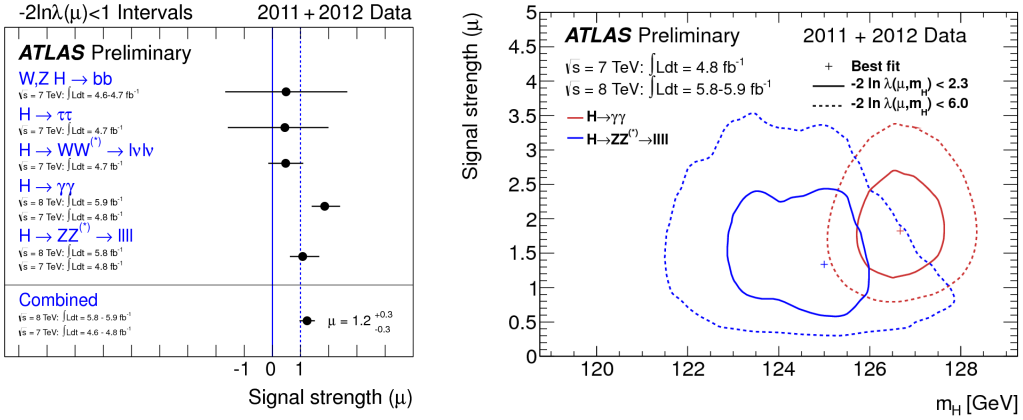

Figure 12: Left: Individual channel and combined fitted signal strength μ values at $m_H = 126.5$ GeV. Right: 2D μ *vs.* m_H contours from independent fits to the $\gamma\gamma$ and 4ℓ data [17].

the $H \to \gamma\gamma$ and $H \to ZZ^{(*)} \to 4\ell$ decay modes. The excesses are compatible with each other and with SM Higgs boson production. The combined search using all data and channels analysed by July 2012 shows an excess with a local significance of 5.0σ at $m_H = 126.5$ GeV. ATLAS therefore reports evidence for a new, narrow resonance at this mass. Exciting times lie ahead, and the collaboration looks forward to adding more channels and the rest of the 2012 LHC dataset to learn more about the nature of this new object.

References

[1] ATLAS Collaboration, ATLAS-CONF-2012-019
[2] CMS Collaboration, CMS PAS HIG-12-008
[3] ATLAS Collaboration, JINST 3 (2008) S08003
[4] ATLAS Collaboration, Phys. Rev. D86 (2012) 032003, arXiv:1207.0319
[5] ATLAS Collaboration, Phys. Rev. Lett. 108 (2012) 111803, arXiv:1202.1414
[6] ATLAS Collaboration, Phys. Lett. B 710 (2012) 383, arXiv:1202.1415
[7] ATLAS Collaboration, Phys. Lett. B 717 (2012) 70, arXiv:1206.2443
[8] ATLAS Collaboration, Phys. Lett. B 717 (2012) 29, arXiv:1205.6744
[9] ATLAS Collaboration, Phys. Lett. B 716 (2012) 62, arXiv:1206.0756
[10] ATLAS Collaboration, submitted to Phys. Lett. B, arXiv:1206.6074
[11] ATLAS Collaboration, JHEP 09 (2012) 070, arXiv:1206.5971
[12] ATLAS Collaboration, submitted to Phys. Lett. B, arXiv:1207.0210
[13] ATLAS Collaboration, ATLAS-CONF-2012-078
[14] ATLAS Collaboration, ATLAS-CONF-2012-094
[15] ATLAS Collaboration, ATLAS-CONF-2012-091
[16] ATLAS Collaboration, ATLAS-CONF-2012-092
[17] ATLAS Collaboration, ATLAS-CONF-2012-093